Geomechanics and Engineering, *Vol. 42, No. 4 (2025) 253-266*
https://doi.org/10.12989/gae.2025.42.4.253

Research on the design method and disaster reduction effect of articulated variable cross-section for sandy tunnel under the action of bedrock normal fault dislocation

Yu Zhang[1a], Shuyuan Xie[1b], Shao An*[2], Lianjin Tao[2c], Xu Zhao[2d] and Qiang Zhang[3e]

[1]*School of Civil and Transportation Engineering, Beijing University of Civil Engineering and Architecture, Beijing, China*
[2]*The Key Laboratory of Urban Security and Disaster Engineering, Ministry of Education, Beijing University of Technology, Beijing, China*
[3]*Beijing Maintenance Group Co., Ltd, Beijing, China*

(*Received March 16, 2025, Revised July 8, 2025, Accepted July 23, 2025*)

Abstract. Tunnel structures that pass through active faults are prone to serious damage under the action of fault displacement. When the tunnel cannot avoid active faults, a series of disaster reduction measures need to be taken to reduce the impact of fault displacement on the tunnel. In current work, firstly, a three-dimensional numerical analysis model was established, and the numerical model was validated through existing centrifugal model experiments. Then, by comparing the damage response of articulated tunnels and integral tunnels under fault action, the energy dissipation mechanism and disaster reduction effect of articulated design method were researched, and the key parameters in the articulated design method, such as the longitudinal position, elastic modulus and length of flexible joint and the length of lining segment, were further analyzed for their influence on the disaster reduction effect. Finally, considering the possibility of groundwater seepage during tunnel operation in areas with abundant water, a variable cross-section disaster reduction method based on the articulated design was proposed, and the disaster reduction effect under different parameter influences were discussed. This work can provide meaningful references for the disaster reduction design method of sand tunnels under the action of bedrock normal fault dislocation.

Keywords: articulation design; bedrock normal fault dislocation; disaster reduction effect; sandy tunnel; variable cross-section

1. Introduction

The damage to underground structures is mainly attributed to the geological vibrations caused by seismic waves and permanent deformation including fault displacements, landslides and ground fissures (Gao *et al.* 2024, Huang *et al.* 2017, Yu *et al.* 2018a, b, Yuan *et al.* 2018, Konagai *et al.* 2005, Liu *et al.* 2018, 2024, Wang *et al.* 2016). Earthquakes usually have a wide range of impacts, but the probability of damage to underground structures is much lower. Permanent geological deformation usually occurs in small areas, but due to large deformations, the possibility and degree of severe damage to underground structures are very high. The significant differential movement on both sides of the fault can cause permanent geological deformation, leading to damage and even collapse of tunnels, buildings, and lifeline engineering (Zaheri *et al.* 2020, Kim *et al.* 2020, Cui *et al.* 2023). In theory, fault zones should be avoided as much as possible in underground structure route planning. However, with the rapid development of tunnel engineering in various countries around the world, and limited by geological conditions, fault locations, and construction costs, faults are inevitable in the planning and design of tunnel engineering (Wang *et al.* 2001, An *et al.* 2021). Therefore, minimizing the impact of fault displacement on tunnel structures through effective engineering measures is a huge challenge faced by designers at present.

The influence of the movement of active faults on underground structures is mainly manifested in two categories: (i) Fault movement propagates from bedrock to the ground surface, causing significant surface rupture and deformation, thereby posing a serious threat to underground structures within the affected area (Agalianos *et al.* 2020, Cole and Lade 1984, Lin *et al.* 2006, Ahmadi *et al.* 2018, Tali *et al.* 2019, Burridge *et al.* 1989, Baziar *et al.* 2014, Liu *et al.* 2015, Cai *et al.* 2019, Kiani *et al.* 2016a, b, Sabagh and Ghalandarzadeh 2020, An *et al.* 2021, Del Amo *et al.* 2018, Anastasopoulos *et al.* 2008a, b); (ii) The underground structure directly crosses the fault fracture zone at the bedrock, causing severe structural damage due to fault displacement (Zhong *et al.* 2020, Shen *et al.* 2014. 2020, Fan *et al.* 2020, Roy and Sarkar 2017, Yu *et al.* 2016, 2013, Lai *et al.* 2017, Zhang *et al.* 2019, Zhao *et al.* 2023, Zhang *et al.* 2024).

At present, scholars have conducted extensive engineering practice, theoretical analysis, numerical

*Corresponding author, Ph.D.
E-mail: as56913@163.com
[a]Ph.D.
[b]Ph.D. Student
[c]Ph.D.
[d]Ph.D.
[e]Ph.D.

ISSN: 2005-307X (Print), 2092-6219 (Online)

simulation, and model experiments to address the above two types of issues. Based on this, a series of anti-fault design methods and engineering measures for crossing active faults have been developed, such as articulated design (Eissenberg and Treadwell 1982, Russo and Germani 2002, Shahidi and Vafaeia 2005, Jalali 2018, Wang *et al.* 2023, Yan *et al.* 2022, 2020), over-excavation design (Caulfield *et al.* 2005), and new material design (Zeng *et al.* 2021, Zhao *et al.* 2019). Articulation design is the most widely used anti-fault measure in existing engineering projects. Its design concept is to divide the continuous tunnel into independent lining segments of a certain length within a certain distance on both sides of the fault, and fill flexible materials with lower stiffness between adjacent lining segments to increase the overall flexibility of the tunnel structure in the affected area of fault movement. For example, in order to reduce the impact of fault displacement, a special seismic joint was installed every 6 meters within a range of approximately 366 meters on both sides of the fault fracture zone in the San Francisco Marine Drainage Project constructed in 1981. Each seismic joint is allowed to undergo 0.3 m tensile deformation, 0.13 m compressive deformation, and 2.4° rotational deformation (Eissenberg and Treadwell 1982). During the construction of Bolu Tunnel in Turkey, in order to deal with the threat of faults, 80 cm fiber concrete is set between the lining and the outer lining, and 0.5 m ~ 0.7 m wide connection joint was set every 4.4 m along the longitudinal direction of the tunnel (Russo and Germani 2002). To reduce the impact of the Zarab fault on the Koohrang-III water conveyance tunnel in Iran, Shahidi and Vafaeian (2005) proposed an articulated design for tunnel lining in fault zones, with plastic concrete flexible materials filled between lining segments to adapt to deformation caused by fault displacement, and the numerical methods were used to determine the length of lining segments and the width of flexible connections. In project of Karaj water conveyance tunnel crossing Pourkan-Verdij fault in Iran, the concrete lining within the affected area of the fault is divided into segments of 1.3 m length, and the joints between the segments are sealed to cope with the possible movement of the active fault (Jalali 2018). Wang *et al.* (2023) studied the mechanical response and failure mechanism of a comprehensive pipe gallery considering flexible joints through the model tests. Yan *et al.* (2022) established a new simplified mechanical model for flexible joints and proposed a method for estimating the response of tunnels with multiple flexible joints under fault displacement.

Based on the above analysis, it can be seen that scholars have conducted extensive research on the structural mechanics characteristics, damage mechanisms and disaster reduction effects of articulated design. However, current research on the disaster reduction effect of tunnel articulated design in sandy is still limited, and reasonable design parameters need to be further explored. Besides, the conventional method of setting flexible joints has caused problems such as heavy waterproof tape at the joint, difficulty in fixing and installing waterproof tape, difficulty in ensuring waterproof quality, and serious water leakage in water rich areas, which seriously threaten the normal operation of underground structures. Thus, it is urgent to reveal the disaster reduction effect of articulated design in sandy tunnels and further propose articulated design methods that can be used in water rich areas.

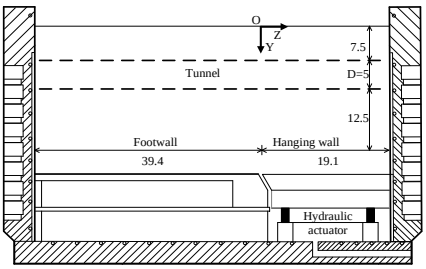

Fig. 1 Elevation view of the model test (all dimensions are in m)

After this introduction, this work is organized as follows: The three-dimensional finite element model was established and validated in Section 2. The energy dissipation mechanism and disaster reduction effect of articulated design method was elaborated in Section 3. The influence of key parameters in articulated design methods was analyzed in Section 4. Moreover, a variable cross-section disaster reduction method based on articulated design principle was proposed in Section 5. Finally, conclusions are summarized in Section 6.

2. Establishment and validation of numerical model

2.1 Establishment of numerical model

Based on centrifuge model test, Cai *et al.* (2019) analyzed the mechanical response characteristics of tunnel under the action of normal fault dislocation in sandy soil. The centrifuge test used a hydraulic loading device to achieve fault dislocation, with a fault inclination angle of 70°, as shown in Fig. 1. Anastasopoulos *et al.* (2008a) have demonstrated that the results obtained using finite element methods in fault dislocation analysis are more in line with model test results. The finite element software ABAQUS was used for numerical simulation in this paper, and a finite element model with dimensions consistent with the prototype size of Cai *et al.* (2019) was established. The dimensions of the established numerical model were 57 m (length) × 18 m (width) × 25 m (depth), as shown in Fig. 2. The outer diameter of the tunnel is 5 m, the thickness is 0.36 m, the burial depth of vault is 7.5 m, and the longitudinal length ratio of the hanging wall and footwall is 1:2. The model parameters were consistent with the centrifuge test conducted by Cai *et al.* (2019), as shown in Table 1. For the model of soil, it should be noted that the Mohr-Coulomb model cannot fully capture the nonlinear behavior of sand and lacks the ability to simulate stiffness variation with depth. However, a large amount of literature has proven that using the Mohr-Coulomb model can effectively simulate the response of overlying soil and tunnel structures under the action of bedrock dislocation (Loukidis *et al.* 2009, Lin *et al.* 2006, 2007, Cai *et al.* 2019, Anastasopoulos *et al.* 2007, Baziar *et al.* 2016). Thus, the

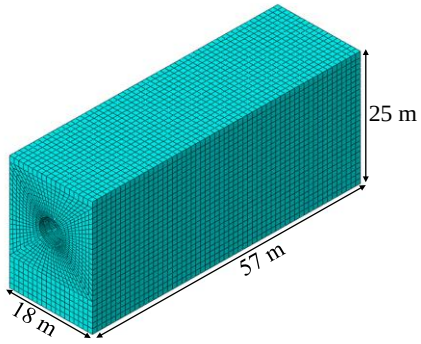

Fig. 2 Three-dimensional finite element model

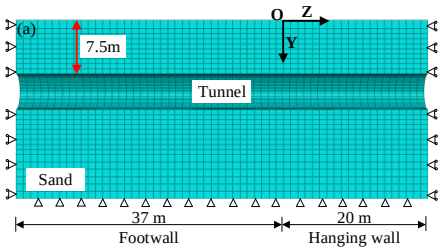

(a) Step 1: balance of self-weight stress

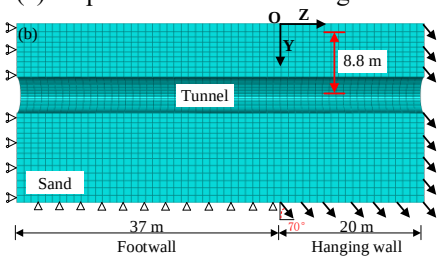

(b) Step 2: apply fault displacement

Fig. 3 Boundary conditions of model

Table 1 Model parameters in numerical simulation

Material	Dry Toyoura sand	Tunnel lining
Elements used	Solid	Solid
Material model	M-C	Linear elastic
Unit weight, γ (kN/m^3)	15.33	25
Cohesion, c (kPa)	0	–
Friction angle, φ (°)	31	–
Dilation angle, ψ (°)	10	–
Elastic modulus, E (MPa)	36	70000
Poisson's ratio, v	0.2	0.35

Mohr-Coulomb model was used for sandy soil, and the linear elastic model was used for tunnel lining. The interface between sand and tunnel adopted hard contact in the normal direction and penalty friction in the tangential direction, with a friction coefficient of 0.24 (Lin *et al.* 2007).

2.2 Simulation process and boundary conditions

The numerical simulation process can be divided into two steps: (1) applying fixed constraints to the bottom of the model and applying normal constraints to the side boundary of the model. Then carry out in-situ stress balance, which is corresponding to the soil self-equilibrium stage in model test; (2) Keep the footwall fixed and apply fault displacement to the bottom and lateral boundaries of the hanging wall, which is corresponding to the stage of fault movement in model test, as shown in Fig. 3.

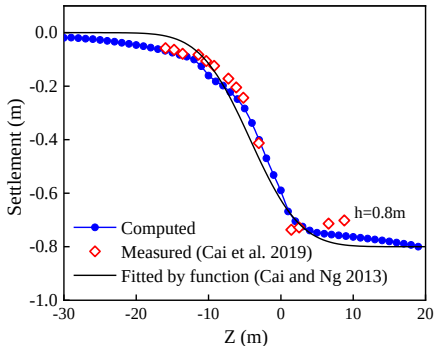

Fig. 4 Ground settlement located at 8.8 m from the tunnel axis

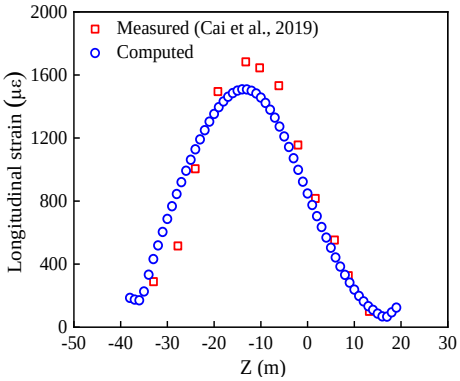

Fig. 5 The comparison of longitudinal strain in tunnel crown

2.3 Model validation

According to the model test of Cai *et al*. (2019), the vertical displacement of 0.8 m and the horizontal displacement of 0.291 m (0.291 m = 0.8 m/tan70°) were applied to the normal fault in the numerical model (see Fig. 3). To verify the correctness of numerical model, Fig. 4 shows the numerical results and model test results of ground settlement at a distance of 8.8 m (see Fig. 3) from the tunnel axis. It is should be noted that the measured settlement can be fitted reasonably through an error function, as suggested by Cai and Ng (2013) for free field conditions

$$V=0.5h\left[erf\left(0.13x+0.55\right)+1\right] \quad (1)$$

The settlement obtained from numerical model is consistent with the measured results and exhibits an error function trend. In addition, the comparison between the longitudinal strain of the tunnel vault and the test results is shown in Fig. 5. It is shown that the maximum longitudinal strain of tunnel vault of numerical simulation and model

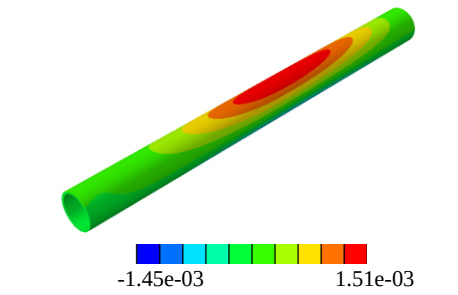

(a) Model length 57 m

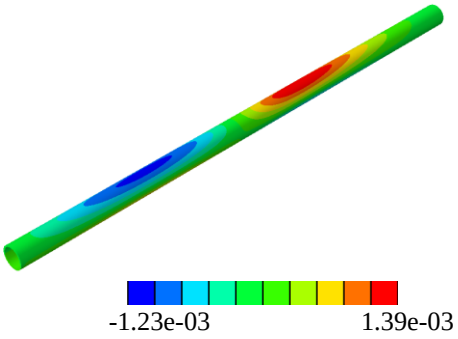

(b) Model length 120 m

Fig. 6 The longitudinal strain contours in tunnel crown of different numerical models

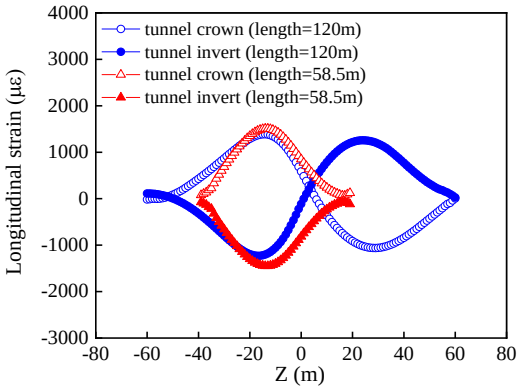

Fig. 7 The longitudinal strain of tunnel crown and invert

test is 1508 με and 1683 με, respectively. The longitudinal strain results of the tunnel vault in numerical simulation are in good agreement with the test results. Thus, it is reasonable to use the above modelling method in the subsequent analysis.

It is worth noting that Sun *et al.* (2019) analyzed the longitudinal strain characteristics of tunnel under the effect of normal faulting by model experiment. The results indicated that the tunnel invert of hanging wall and crown of footwall were in the tensile state, and the tunnel crown of hanging wall and invert of footwall were in the compressive state. However, when the longitudinal length of the numerical model is 57 m, only the tunnel crown and invert strain state of footwall is reflected (see Fig. 5). Thus, the longitudinal length of the numerical model is increased to 120 m to comprehensively reflect the longitudinal response of the tunnel lining. That is, the numerical model size is ultimately determined to be 120 m (length) × 30 m (width) × 25 m (depth). The length ratio of hanging wall and footwall is 1:1. In addition, Anastasopoulos *et al*. (2007) pointed out that the mesh width in length direction of the model has a significant impact on the calculation results, and determined through parameter analysis that the calculation accuracy can be guaranteed when the mesh width is ≤ 1 m. Thus, to fully consider the calculation accuracy and efficiency, mesh width in the length direction of the calculation model in this paper is set to 1 m. The contours of longitudinal strain of numerical model with length 57 m and 120 m are presented in Fig. 6. The longitudinal strains of tunnel crown and invert are shown in Fig. 7. When the longitudinal length of the numerical model is 120 m, the longitudinal response of the tunnel lining is reflected comprehensively, indicating that the model length of 120 m meets the calculation requirements. With the increase of longitudinal length, the maximum longitudinal strain decreases because the influence of boundary on tunnel response is getting smaller.

For tunnel lining, the elastic model cannot consider the stiffness degradation of concrete during the plastic stage under large deformation, and cannot quantify the degree of damage to tunnel lining. Thus, the Concrete Plastic Damage Model (CDP) is used to simulate tunnel damage under normal fault dislocation. In the numerical model, the tunnel lining is set to C30, with a density of 2500 kg/m^3, an elastic modulus of 30 GPa, a Poisson's ratio of 0.2, and the plastic damage parameters are shown in Table 2.

3. Energy consumption mechanism and disaster reduction effect of articulated design

3.1 Determination of the length of lining segment and flexible joint

According to the deformation characteristics of the tunnel under fault displacement, Shahidi *et al*. (2005) pointed out that the maximum length of the lining segment should not exceed the distance between the maximum values of positive and negative bending moments. Fig. 8 shows the bending moment and vertical displacement of the arch along the longitudinal direction of the tunnel. It can be seen that the bending moment exhibits an antisymmetric distribution along the longitudinal direction, with drastic changes within a range of 33 m on both sides of the displacement surface, gradually decreasing and stabilizing thereafter. The distance between the maximum values of positive and negative bending moments is defined as L_M, and the length of the lining segment is defined as L_j. Based on the suggestion of Shahidi *et al.* (2005), $L_j \leq L_M$=33 m can be obtained in numerical model.

Fig. 9 shows a schematic diagram of the deformation of the lining based on articulated design under the action of fault displacement from Shahidi and Vafaeian (2005). The relationship between fault vertical displacement Δu, lining segment length L_j, and flexible joint length L_R is

$$L_R = \frac{\Delta u}{\varphi_u L_j} \tag{2}$$

Table 2 Damage parameters of concrete (C30)

Compressive stress (MPa)	Inelastic strain (10^{-3})	Compression damage factor dc	Tensile stress (MPa)	Cracking strain (10^{-3})	Tensile damage factor dt
5.82	0.0000	0.0000	1.26	0.0000	0.0000
20.10	0.8018	0.3577	2.01	0.0282	0.2256
17.91	1.6030	0.5194	1.18	0.1608	0.5462
14.41	2.5196	0.6460	0.81	0.2729	0.7246
11.66	3.4112	0.7315	0.63	0.3789	0.8150
10.11	4.0630	0.7773	0.53	0.4824	0.8661
8.21	5.1264	0.8313	0.46	0.5848	0.8979
6.65	6.3782	0.8735	0.40	0.6866	0.9192
5.29	8.0237	0.9087	0.36	0.7879	0.9341
4.58	9.2474	0.9260	0.33	0.8889	0.9451
4.29	9.8571	0.9329	0.31	0.9897	0.9534

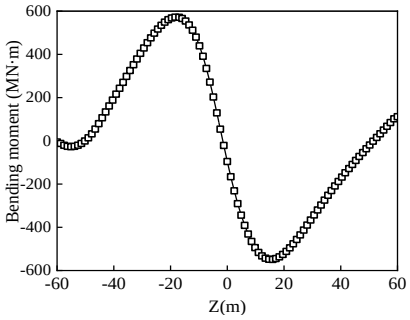

(a) Bending moment

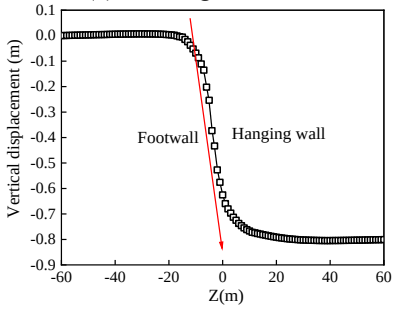

(b) Vertical displacement

Fig. 8 Longitudinal bending moment and vertical displacement of arch crown

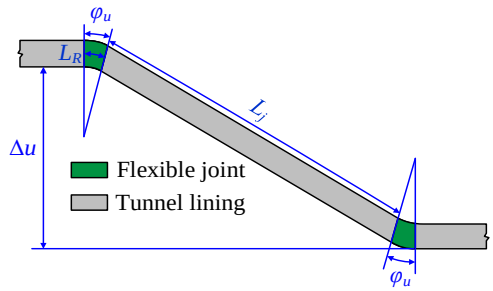

Fig. 9 Deformation of tunnel lining with flexible joints (recreated from Shahidi and Vafaeian (2005))

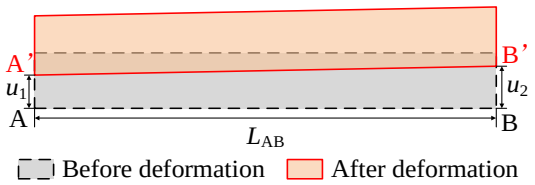

Fig. 10 Schematic diagram of longitudinal angle

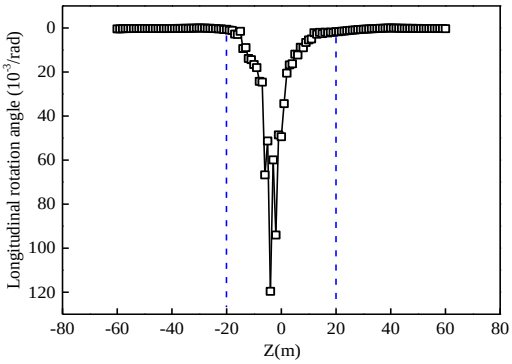

Fig. 11 Longitudinal distribution curve of rotation angle

where φ_u is the ultimate bending curvature of the lining, which can be determined as 0.015 according to the research results of Li (2009).

Considering that the current length of concrete lining trolley is generally 6~12 m, the length of the lining segment L_j in the numerical model is determined to be 12 m. It is assumed that the vertical displacement Δu of the fault is 0.2 m, and the length of flexible joint L_R can be obtained from Eq. (2) as 1 m.

To determine the total length of longitudinal fortification, the longitudinal rotation angle of the tunnel is defined as the change in vertical displacement per meter along the tunnel axis, as shown in Fig. 10. Points A and B are the initial positions of the tunnel, and the distance between AB is L_{AB}. After the fault displacement, the positions of the tunnel after deformation are A 'and B', respectively. The vertical displacement of AA' is u_1, and the vertical displacement of BB' is u_2. Therefore, the expression for the longitudinal angle θ of the tunnel is expressed as

$$\theta = \frac{u_2 - u_1}{L_{AB}} \tag{3}$$

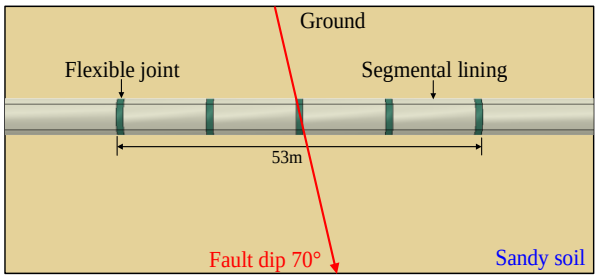

Fig. 12 Longitudinal layout of flexible joint

Table 3 Material parameters of flexible joint

Material	Unit weight γ (kN/m^3)	Elastic modulus E (MPa)	Poisson's ratio v
Flexible joint	1.0	7.8	0.47

Fig. 11 depicts the distribution curve of the longitudinal rotation angle of the tunnel. It is shown that the deformation of the tunnel is mainly concentrated at the horizontal axis of -20 m to 20 m. The maximum longitudinal angle of the lining during fault displacement occurs at the horizontal axis of -5 m, therefore a flexible joint is set up here.

Considering the influence range of fault displacement on the tunnel, the layout of segmented lining is carried out within the range of -31 m to 22 m on the horizontal axis. The total length of the articulated design is determined to be 53 m, and the longitudinal layout is shown in Fig. 12.

3.2 Flexible joint parameters

As a flexible connecting material, it should have high tensile strength and toughness characteristics, so as to ensure that brittle failure does not occur when the strain is large, and continue to maintain a certain level of strength and waterproofing. In numerical model, considering the good toughness of flexible connection material, it can be simulated as elastic model, and the tied connection is used between the flexible joint and the lining segment. The parameters of flexible materials are shown in Table 3.

3.3 Analysis of energy consumption mechanism in articulated design

Fault dislocation is essentially a process of energy release. According to the law of conservation of energy, various energies within the model structure are converted into each other. The numerical cases of the integrated tunnel and the segmented articulated tunnel were set, and a vertical displacement of 0.2 m and a horizontal displacement of 0.073 m were applied to the hanging wall. The energy released by fault dislocation can cause damage to the structure, so the disaster reduction mechanism of the articulated design method can be explained from the perspective of structural damage energy dissipation.

Fig. 13 depicts the comparison of damage energy consumption between articulated design and integral tunnels. The damage energy consumption of both integral and articulated tunnels increases with the increase of fault

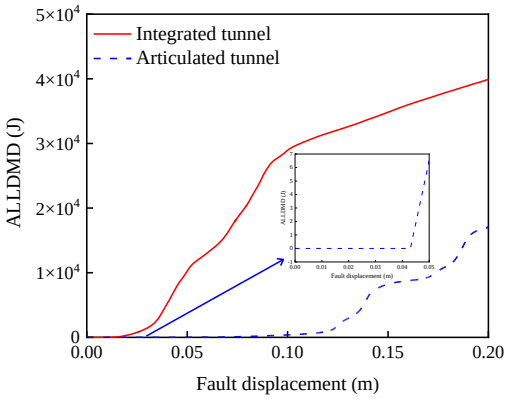

Fig. 13 Comparison of damage energy consumption between articulated tunnel and integrated tunnel

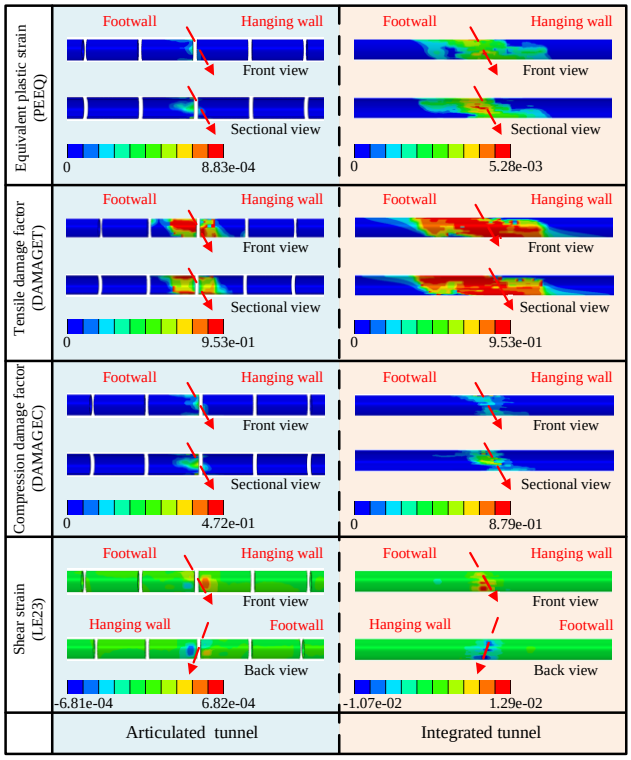

Fig. 14 Longitudinal layout of flexible joint

displacement. When the damage energy consumption is 0, it indicates that the tunnel structure is still in the elastic state, while when the damage energy consumption is greater than 0, it indicates that the tunnel structure has been damaged. The fault displacement at the beginning of damage in the integrated tunnel and the articulated tunnel is 0.01 m and 0.043 m, respectively. After damage occurs to the tunnel structure, the damage energy consumption of integral tunnel increases rapidly, while the damage energy consumption of articulated tunnel shows an extremely slow growth trend. This is because the flexible joint of the articulated design absorbs the energy of fault displacement on the lining structure through its own deformation, proving that the articulated design has a significant disaster reduction effect on tunnel damage caused by normal fault dislocation.

Table 3 Material parameters of flexible joint

Cases	Longitudinal position of flexible joint	Elastic modulus of flexible joint E_j (MPa)	Length of lining section L_R (m)	Length of flexible joint L_j (m)
1	Through flexible joint	7.8	12	1
2	Through the midpoint of the lining segment	7.8	12	1
3	Through flexible joint	78	12	1
4	Through flexible joint	780	12	1
5	Through flexible joint	7.8	4	1
6	Through flexible joint	7.8	8	1
7	Through flexible joint	7.8	12	0.5
8	Through flexible joint	7.8	12	1.5

3.4 Disaster reduction effect of articulated tunnel

Fig. 14 shows the comparison of the structural damage nephogram of the integrated tunnel and the segmented articulated tunnel. The equivalent plastic strain (PEEQ) of the tunnel is distributed from the vault of footwall to the arch bottom of hanging wall, and the distribution trend is consistent with the normal fault dislocation trajectory. The maximum PEEQ of the integrated tunnel is 5.277×10^{-3}, which occurs at the arch waist at the longitudinal coordinate of -5 m. The maximum PEEQ of the articulated tunnel is 8.826×10^{-4}, which is 83.27% lower than that of the integrated tunnel. The range of PEEQ in segmented articulated tunnel is significantly reduced and mainly concentrated near the articulated joints.

When C30 concrete reaches its ultimate tensile and compressive strength (2.01 MPa and 20.1 MPa), the corresponding tensile and compressive damage factors are 0.2256 and 0.3577, respectively. Thus, it can be simply assumed that the tensile damage factor (DAMAGET) ≥ 0.2256 is the tensile damage element, and the compressive damage factor (DAMAGEC) ≥ 0.3577 is the compressive damage element. In the integrated tunnel, the volumes of tensile and compressive damage are 146.47 m^3 and 13.5 m^3 respectively, and the range of tensile damage is greater than that of compressive damage. Although the maximum DAMAGET of both articulated and integrated tunnel is 0.953, the tensile damage volume of articulated tunnel is 61.78 m^3, which is 57.74% lower than that of integrated tunnel. The maximum DAMAGEC and compression damage volume of the articulated tunnel are 0.472 and 0.32 m^3, respectively, which are 46.31% and 97.6% lower than those of the integrated tunnel.

The shear strain is symmetrically distributed along the longitudinal axis of the tunnel, and the maximum shear strain occurs at the arch waist or arch foot. The maximum shear strain of integrated tunnel is 1.29×10^{-2}, while the maximum shear strain of the articulated tunnel is 6.82×10^{-4}, which is 94.72% lower than that of integrated tunnel. From the above analysis, it can be concluded that the setting of flexible joints in articulated tunnel can help the lining structure better adapt to the deformation caused by faults, thereby effectively reducing the damage of fault displacement to the structure.

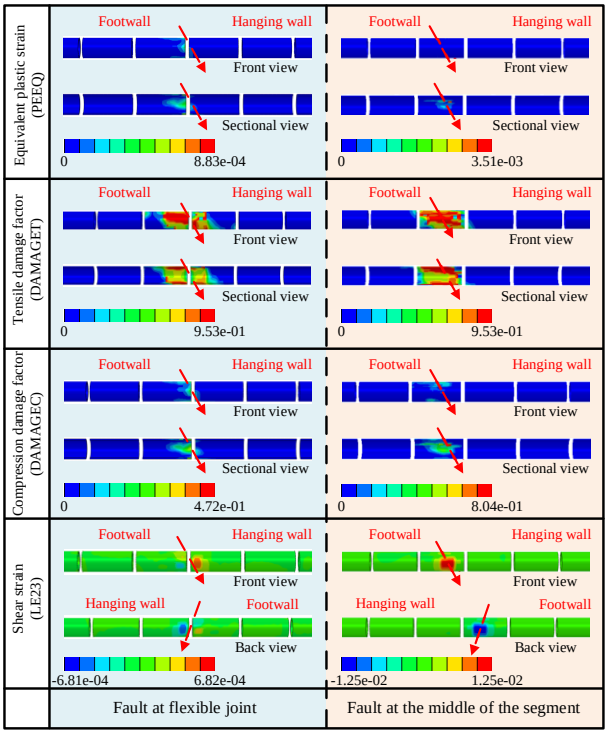

Fig. 15 Contours of various damage indicators under different positions of flexible joint

4. Analysis of key parameters of articulated tunnel

In this Section, sensitivity analysis was conducted on the impact of key parameters in articulated tunnels on disaster reduction effectiveness, such as the longitudinal position of flexible joints, the elastic modulus of flexible joints, the length of lining segments, and the length of flexible connections. The cases are shown in Table 4.

4.1 Longitudinal position of flexible joints

Considering that the longitudinal position relationship between the fault displacement surface and the flexible joint may have an impact on the degree of tunnel damage, the fault displacement surface is set at flexible joint (case 1) and the midpoint of the lining segment (case 2), respectively. Apply a vertical displacement of 0.2 m and a horizontal displacement of 0.073 m to the fault. The comparison of damage nephogram and indicator values for lining in cases 1 and 2 is shown in Figs. 15 and 16, respectively.

It is shown that compared with the integrated tunnel, the maximum PEEQ of the lining structure in case 2 is 3.512×10^{-3}, which is reduced by 33.4%; the maximum shear strain is 1.251×10^{-2}, which is reduced by 3%; The maximum DAMAGET is 0.953, which is equal to the result of the integrated tunnel; the tensile damage volume is 61.8m^3, which is reduced by 57.8%; The maximum DAMAGEC is 0.8, which is reduced by 8.3%; and the compression damage volume is 3.0m^3, which is reduced by 76.9%.

Compared with the results of case 1, the maximum

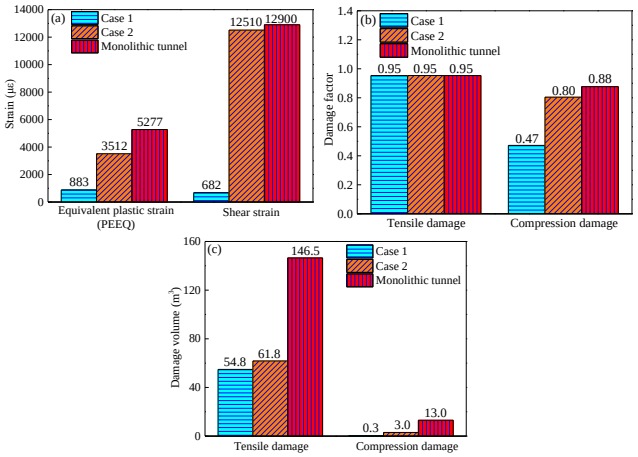

Fig. 16 Comparison of damage indicators and volumes under different positions of flexible joint

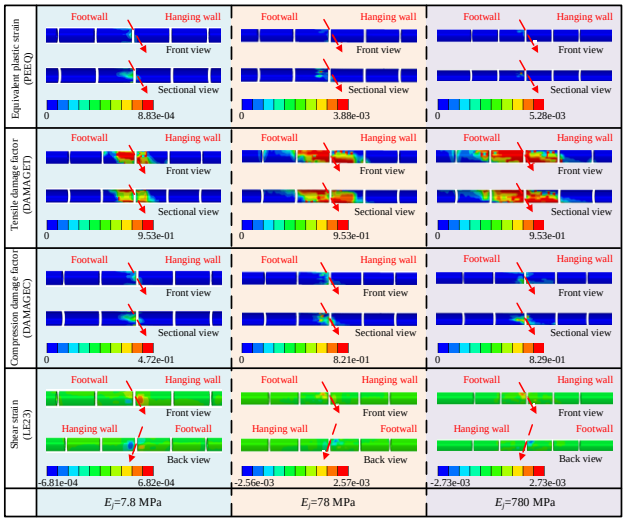

Fig. 17 Contours of various damage indicators under different elastic modulus of flexible joint

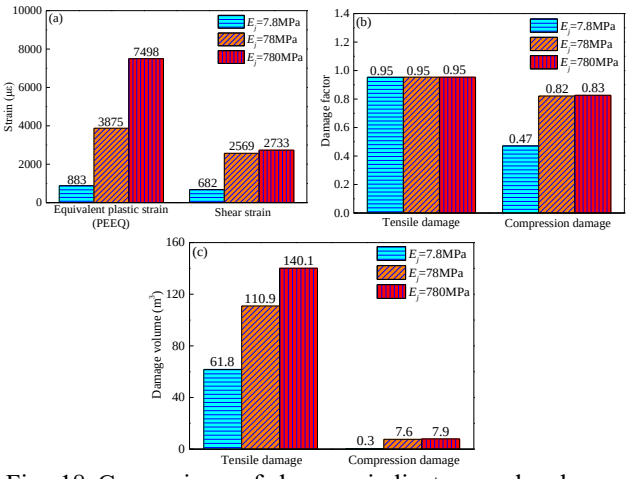

Fig. 18 Comparison of damage indicators and volumes under different elastic modulus of flexible joint

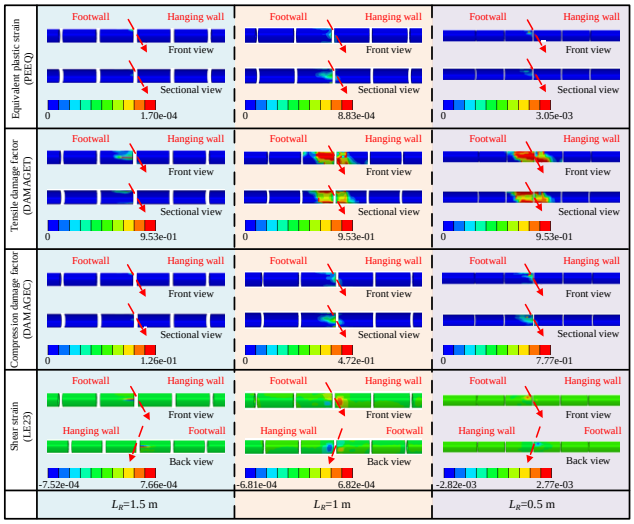

Fig. 19 Contours of various damage indicators under different length of flexible joint

PEEQ of the lining structure in case 2 increased by 297.9%; the maximum shear strain increased by 1735.7%; the maximum DAMAGET is equal, and the volume of tensile damage increased by 13.0%; the maximum DAMAGEC increased by 70.45%, and the compressive damage volume increased by 840.6%.

According to the above analysis, it can be concluded that the degree and volume of tunnel damage in case 2 are higher than those in case 1. The reason for this phenomenon is that when the flexible joint is set at the most unfavorable position of fault dislocation, it can maximize the consumption of energy generated by fault dislocation and significantly reduce the shear strain of the tunnel. When the fault displacement surface passes through the midpoint of the lining segment, the shear strain of the tunnel is reduced compared to the integrated tunnel, but the reduction is not significant. Therefore, flexible joint should be set at the position of fault dislocation position to minimize the damage to the tunnel.

4.2 Elastic modulus of flexible joint

Take the elastic modulus E_j of the flexible joint as 7.8 MPa, 78 MPa and 780 MPa respectively, and apply a vertical displacement of 0.2 m and a horizontal displacement of 0.073 m to the normal fault. The comparison of damage nephogram and indicator values for lining structure under different elastic modulus of flexible joint is shown in Figs. 17 and 18, respectively.

Compared with the case of E_j=7.8 MPa, the maximum PEEQ of the lining structure under the case of E_j=78 MPa and E_j=780 MPa are 3.875×10^{-3} and 7.498×10^{-3} respectively, which are increased by 339.04% and 749.53%; The maximum shear strain are 2.569×10^{-3} and 2.733×10^{-3} respectively, which are increased by 276.96% and 301.03%; The maximum DAMAGET are both 0.95, and the tensile damage volumes are 110.9 m^3 and 140.1 m^3 respectively, which are increased by 79.49% and 126.83%; The maximum DAMAGEC are 0.82 and 0.83 respectively, and the compression damage volumes are 7.6 m^3 and 7.9 m^3 respectively, which are increased by 2281.25% and 2381.25%. From the above analysis, it is shown that as the elastic modulus of the flexible joint decreases, the degree of

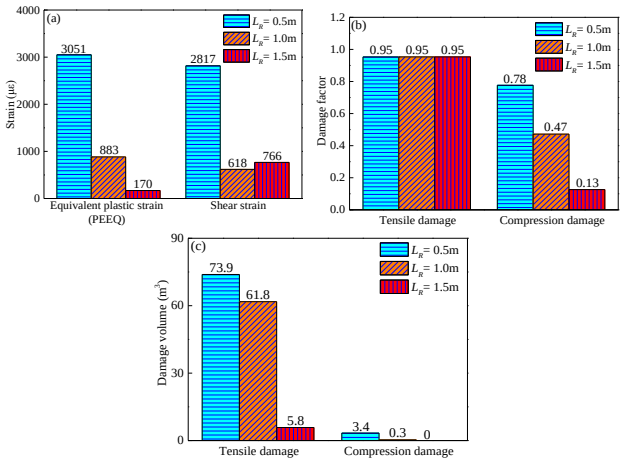

Fig. 20 Comparison of damage indicators and volumes under different length of flexible joint

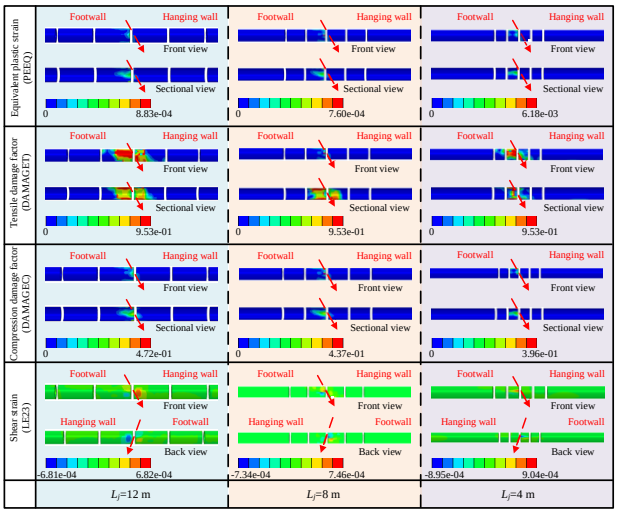

Fig. 21 Contours of various damage indicators under different length of lining segment

tunnel damage and volume also decrease. This is because the lower the elastic modulus of the flexible joint, the more deformation under fault displacement is absorbed by the flexible joint.

4.3 Length of flexible joint

Take the length L_R of the flexible joint as 0.5 m, 1 m and 1.5 m respectively, and apply a vertical displacement of 0.2 m and a horizontal displacement of 0.073 m to the normal fault. The comparison of damage nephogram and indicator values for lining structure under different length of flexible joint is shown in Figs. 19 and 20, respectively.

In case of L_R=0.5 m, the maximum PEEQ, maximum shear strain, maximum DAMAGET, tensile damage volume, maximum DAMAGEC and compression damage volume are 3.051×10^{-3}, 2.817×10^{-3}, 0.95, 73.9 m^3, 0.78 and 3.4 m^3, respectively. Compared with the case of L_R=0.5 m, the maximum PEEQ under the case of L_R=1 m and L_R=1.5 m are 8.83×10^{-4} and 1.7×10^{-4} respectively, which are reduced by 71.07% and 94.44%; The maximum shear strain are 6.18×10^{-4} and 7.66×10^{-4} respectively, which are reduced by 78.04% and 73.02%; The maximum DAMAGET are both 0.95, and the tensile damage volumes are 61.8 m^3 and 5.8 m^3 respectively, which are reduced by 16.39% and 92.14%; The maximum DAMAGEC are 0.47 and 0.13 respectively, and the compression damage volumes are 0.3 m^3 and 0 m^3 respectively, which are reduced by 90.44% and 100%. Thus, as the length of the flexible joint increases, the degree and volume of tunnel damage decrease.

4.4 Length of lining segment

Take the length L_j of the lining segment as 4 m, 8 m and 12 m respectively, and apply a vertical displacement of 0.2 m and a horizontal displacement of 0.073 m to the normal fault. The comparison of damage nephogram and indicator values for lining structure under different length of lining segment is shown in Figs. 21 and 22, respectively.

Compared with the case of L_j=12 m, the maximum PEEQ under the case of L_j=8 m and L_j=4 m are 8.83×10^{-4}

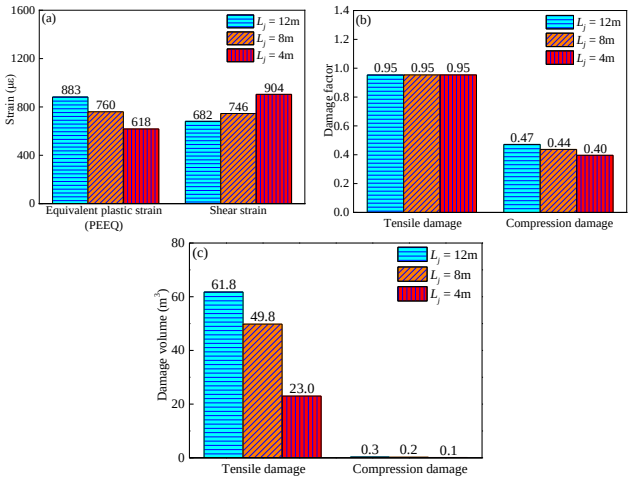

Fig. 22 Comparison of damage indicators and volumes under different length of lining segment

and 1.7×10^{-4} respectively, which are reduced by 13.89% and 30%; The maximum shear strain are 7.46×10^{-4} and 9.04×10^{-4} respectively, which are increased by 20.56% and 46.34%; The maximum DAMAGET are both 0.95, and the tensile damage volumes are 49.83 m^3 and 22.99 m^3 respectively, which are reduced by 19.34% and 62.79%;The maximum DAMAGEC are 0.44 and 0.4 respectively, and the compression damage volumes are 0.2 m^3 and 0.1 m^3 respectively, which are reduced by 31.25% and 62.5%. Based on the above analysis, it can be concluded that as the length of the lining segment decreases, the degree and volume of tunnel damage also decrease. Therefore, the length of the flexible lining segment should be selected as short as possible.

5. Design method for articulated variable cross-section

According to the analysis in Section 4, the lower the stiffness of the flexible joint, the shorter the length of the

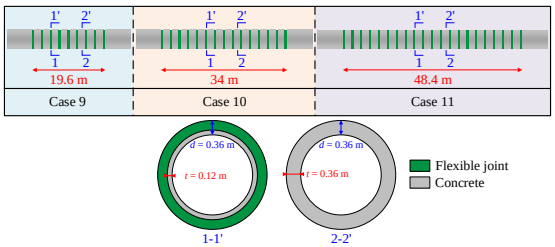

Fig. 23 Schematic diagram of different longitudinal fortification length

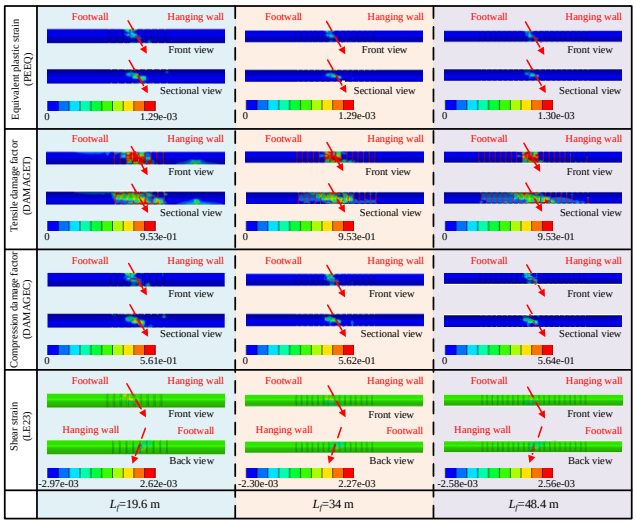

Fig. 24 Contours of various damage indicators under different longitudinal fortification length

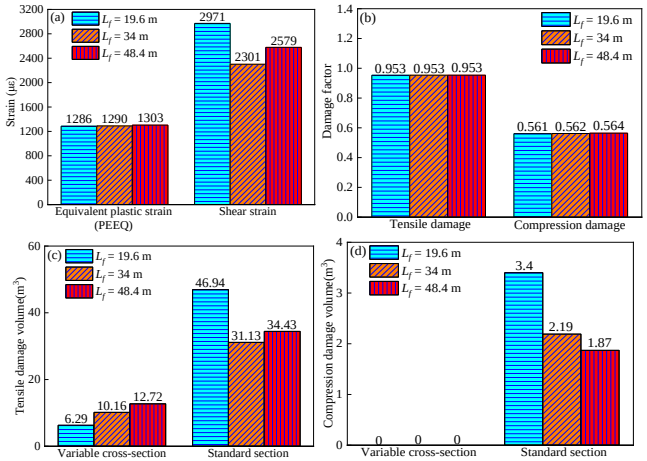

Fig. 25 Comparison of damage indicators and volumes under different longitudinal fortification length

lining segment, and the longer the length of the flexible joint, the smaller the damage and failure of the tunnel under the action of fault displacement. Therefore, it is generally recommended to choose shorter lining segments for tunnels crossing active faults. However, choosing shorter lining segments means setting multiple joints in the tunnel, which may lead to groundwater leakage during normal operation in water rich areas. Therefore, in order to solve the possible problem of groundwater leakage, a variable cross-section disaster reduction method based on the articulated design is proposed in this paper. The disaster reduction principle of this method is to change the thickness of concrete at the variable cross-section and fill it with flexible materials to reduce stiffness, thereby reducing tunnel damage caused by fault displacement. Besides, the integrity of the tunnel can be maintained to reduce the possibility of groundwater leakage during the operation phase. In order to evaluate the effectiveness of the variable cross-section disaster reduction method based on articulated design proposed in this paper, numerical analysis was conducted on its key parameters, such as longitudinal fortification length, lining structure thickness and position.

5.1 Longitudinal fortification length of variable cross-section

The lining thickness at the variable cross-section of the tunnel is taken as 0.12 m (1/3 of the thickness of the standard cross-section), and the other 2/3(0.24 m) are filled with flexible materials. The variable section length and lining segment length are taken as 0.4 m and 2 m, respectively. 3 cases were set with longitudinal fortification lengths of 19.6 m, 34 m, and 48.4 m, as shown in Fig. 23. Apply a vertical displacement of 0.2 m and a horizontal displacement of 0.073 m to the normal fault. The comparison of damage nephogram and indicator values for lining structure under different longitudinal fortification lengths is shown in Figs. 24 and 25, respectively.

Compared with the calculation results of the integral tunnel, the maximum PEEQ of the case 9, 10 and 11 are 1.286×10^{-3}, 1.29×10^{-3} and 1.303×10^{-3}, which are reduced by 75.63%, 75.55% and 75.31%; The maximum shear strain are 2.971×10^{-3}, 2.301×10^{-3} and 2.578×10^{-3}, which are reduced by 76.97%, 82.16% and 80.02%; The maximum DAMAGET are both 0.95; The tensile damage volumes at the variable cross-section are 6.29 m^3, 10.16 m^3, and 12.72 m^3, respectively, while the tensile damage volumes at the standard cross-section are 46.94 m^3, 31.13 m^3, and 34.43 m^3, respectively; The maximum DAMAGEC are 0.561, 0.562 and 0.564 respectively, and the compression damage volumes are 3.4 m^3, 2.19 m^3 and 1.87 m^3 respectively.

The maximum values of various damage indicators of the lining are basically the same under different fortification lengths, and the main damage at the variable cross-section is tensile or shear failure. The total tensile damage volume in cases 9, 10, and 11 is 53.23 m^3, 41.29 m^3, and 47.15 m^3, respectively. It is shown when using the variable cross-section design method, the longitudinal fortification length should be accurately determined. If the fortification length is too long or too short, it will cause an increase in the tensile damage volume to the lining.

5.2 Lining thickness at variable cross-section

The longitudinal fortification length at the variable cross-section is taken as 34 m, and the concrete thickness at the variable cross-section is 0.12 m, 0.24 m, and 0.36 m (Corresponding to integral tunnel), respectively, as shown in Fig. 26. Apply a vertical displacement of 0.2 m and a horizontal displacement of 0.073 m to the normal fault. The comparison of damage nephogram and indicator values for

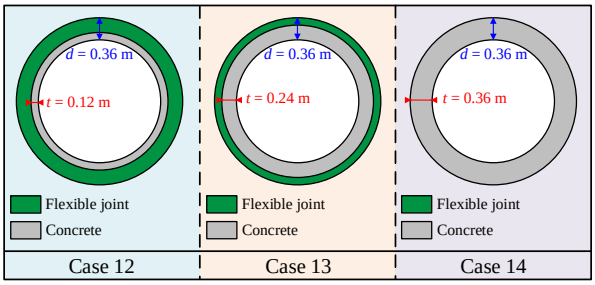

Fig. 26 Schematic diagram of different lining thickness

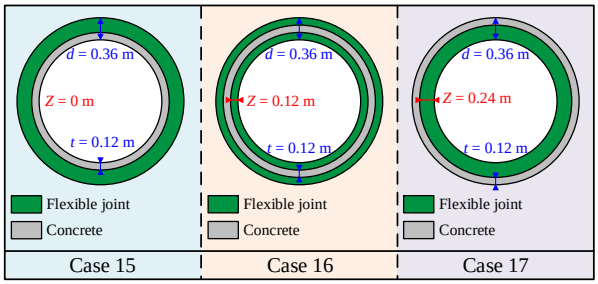

Fig. 29 Schematic diagram of different lining position

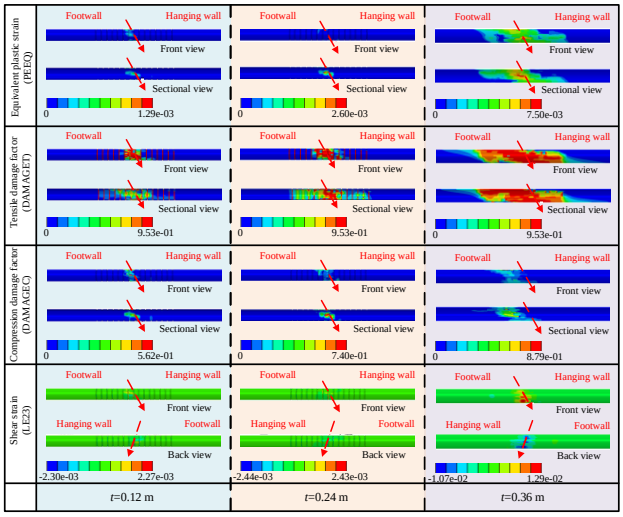

Fig. 27 Contours of various damage indicators under different lining thickness

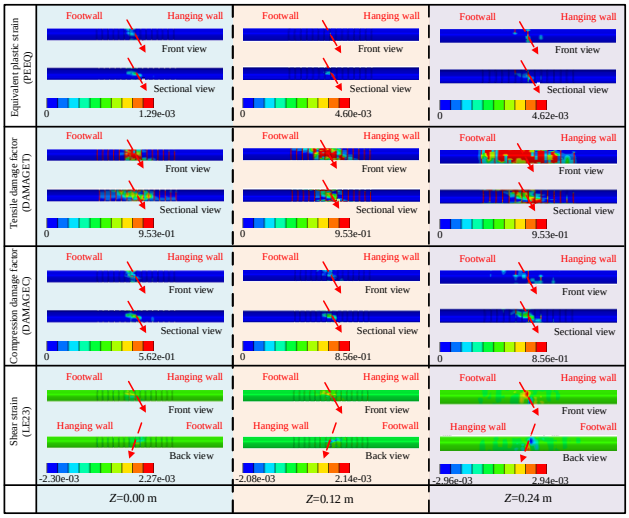

Fig. 30 Contours of various damage indicators under different lining position

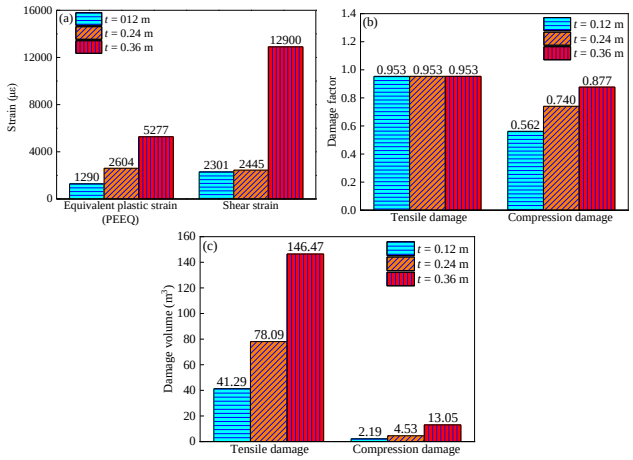

Fig. 28 Comparison of damage indicators and volumes under different lining thickness

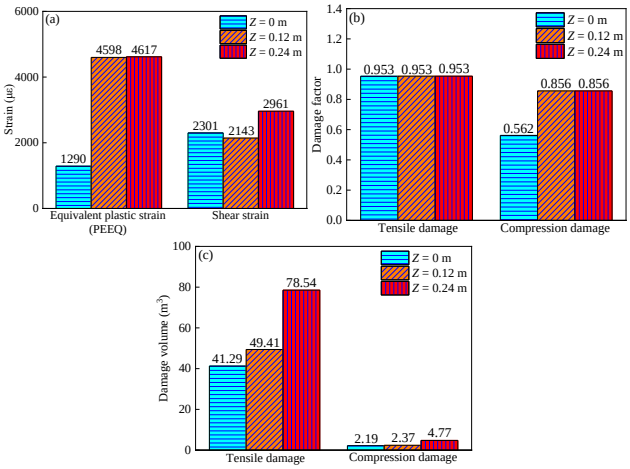

Fig. 31 Comparison of damage indicators and volumes under different lining position

lining structure under different lining thickness is shown in Figs. 27 and 28, respectively.

Compared with the case of t=0.12 m, the maximum PEEQ under the case of t=0.24 m and t=0.36 m are 2.604×10^{-3} and 5.277×10^{-3} respectively, which are increased by 101.86% and 309.07%; The maximum shear strain are 2.445×10^{-3} and 1.29×10^{-2} respectively, which are increased by 6.23% and 460.63%; The maximum DAMAGET are both 0.95, and the tensile damage volumes are 78.09 m^3 and 146.47 m^3 respectively, which are increased by 89.13% and 254.73%; The maximum DAMAGEC are 0.74 and 0.88 respectively, and the compression damage volumes are 4.53 m^3 and 13.05 m^3 respectively, which are increased by 106.86% and 495.89%. Therefore, as the thickness of the lining at the variable cross-section increases, the disaster reduction effect gradually decreases.

5.3 Lining position at variable cross-section

On the basis of a longitudinal fortification length of 34 m and a lining thickness of 0.12 m at the variable cross-

section, the lining is set at different positions at the variable cross-section (Z=0 m, 0.12 m, and 0.24 m), as shown in Fig. 29. That is, the lining gradually changes from the inner side to the outer side of the section. Apply a vertical displacement of 0.2 m and a horizontal displacement of 0.073 m to the normal fault. The comparison of damage nephogram and indicator values for lining structure under different lining position is shown in Figs. 30 and 31, respectively.

Compared with the case of Z=0 m, the maximum PEEQ under the case of Z=0.12 m and Z=0.24 m are 4.598×10^{-3} and 4.617×10^{-3} respectively, which are increased by 256.43% and 257.91%; The maximum shear strain are 2.143×10^{-3} and 2.961×10^{-3} respectively, which are increased by -6.87% and 28.68%; The maximum DAMAGET are both 0.953, and the tensile damage volumes are 49.41 m^3 and 78.54 m^3 respectively, which are increased by 19.67% and 90.21%; The maximum DAMAGEC are both 0.856, and the compression damage volumes are 2.37 m^3 and 4.27 m^3 respectively, which are increased by 8.22% and 94.98%. It is obvious that as the lining is gradually arranged towards the outer diameter, the disaster reduction effect gradually decreases.

6. Conclusions

In this work, based on the finite element analysis method, the energy dissipation mechanism of articulated design was revealed, and the influence of the relative position between the fault displacement surface and the flexible joint, the elastic modulus of the flexible joint, the length of the lining segment and the length of the flexible joint on the disaster reduction effect of the lining structure were studied. Finally, a variable cross-section disaster reduction method based on the articulated design was proposed to address the issue of water leakage that may occur during the operation phase of segmental tunnel, and parameter analysis was carried out on the disaster reduction effect of the thickness and position of the structure at the variable cross-section. The following conclusions can be drawn:

(1) The deformation of flexible joints can effectively consume the energy of fault displacement and reduce the damage to lining structures. When the flexible joint coincides with the fault displacement surface, the flexible joint can maximize the consumption of fault displacement energy and achieve the best disaster reduction effect. When the fault displacement surface coincides with the midpoint of the lining segment, the disaster reduction effect of the tunnel is not significant.

(2) The lower the elastic modulus of the flexible joint, the shorter the length of the lining segment, and the longer the length of the flexible joint, the better the disaster reduction effect of the lining structure.

(3) The variable cross-section anti fracture design method is essentially an evolution of the articulated design method, which has a good disaster reduction effect on fault displacement. Although the disaster reduction effect of the variable cross-section design method is inferior to the method of using flexible joints for the entire cross-section, the use of variable section design can reduce the possibility of water leakage in tunnels during operation.

(4) When using variable cross-section for lining design, the disaster reduction effect gradually decreases with the increase of cross-section thickness. As the lining gradually changes from the inner side to the outer side at the variable cross-section, the disaster reduction effect gradually decreases.

Acknowledgments

The research described in this paper was financially supported by the National Natural Science Foundation of China (42402283) and R&D Program of Beijing Municipal Education Commission (KM202410016016). These financial supports are gratefully acknowledged.

References

Agalianos, A., Sieber, M. and Anastasopoulos, I. (2020), "Cost-effective analysis technique for the design of bridges against strike-slip faulting", *Earthq. Eng. Struct. D.*, **49**(11), 1137-1157. https://doi.org/10.1002/eqe.3282.

Ahmadi, M., Moosavi, M. and Jafari, M.K. (2018), "Experimental investigation of reverse fault rupture propagation through wet granular soil", *Eng. Geol.*, **239**, 229-240. https://doi.org/10.1016/j.enggeo.2018.03.032.

Anastasopoulos, I., Gazetas, G., Bransby, M.F., Davies, M.C.R. and El Nahas, A. (2007), "Fault rupture propagation through sand: finite-element analysis and validation through centrifuge experiments", *J. Geotech. Geoenviron. Eng.*, **133**(8), 943-958. https://doi.org/10.1061/(ASCE)1090-0241(2007)133:8(943).

Anastasopoulos, I., Callerio, A., Bransby, M.F., Davies, M.C.R., Nahas, A.E., Faccioli, E. and Gazetas, G. (2008a), "Numerical analyses of fault-foundation interaction", *Bull. Earthq. Eng.*, **17**(6), 645-675. https://doi.org/10.1007/s10518-008-9078-1.

Anastasopoulos, I., Gerolymos, N., Drosos, V., Georgarakos, T., Kourkoulis, R. and Gazetas, G. (2008b), "Behavior of deep immersed tunnel under combined normal fault rupture deformation and subsequent seismic shaking", *Bull. Earthq. Eng.*, **6**(2), 213-239. https://doi.org/10.1007/s10518-007-9055-0.

An, S., Tao, L.J., Han, X.C. and Zhang, Y. (2021), "Application of two-level design method on subway tunnel crossing active fault: a case study on Urumqi subway tunnel intersected by reverse fault dislocation", *Bull. Eng. Geol. Environ.*, **80**, 3871-3884. https://doi.org/10.1007/s10064-021-02164-y.

Baziar, M.H., Nabizadeh, A., Lee, C.J. and Hung, W.Y. (2014), "Centrifuge modeling of interaction between reverse faulting and tunnel", *Soil Dyn. Earthq. Eng.*, **65**, 151-164. https://doi.org/10.1016/j.soildyn.2014.04.008.

Baziar, M.H., Nabizadeh, A., Mehrabi, R., Lee, C.J. and Hung, W.Y. (2016), "Evaluation of underground tunnel response to reverse fault rupture using numerical approach", *Soil Dyn. Earthq. Eng.*, **83**, 1-17. https://doi.org/10.1016/j.soildyn.2015.11.005.

Burridge, P.B., Scott, R.F. and Hall, J.F. (1989), "Centrifuge study of faulting effects on tunnel", *J. Geotech. Eng.*, **115**(7), 949-967.

Cai, Q.P., Peng, J.M., Charles, W.W., Shi, J.W. and Chen, X.X. (2019), "Centrifuge and numerical modelling of tunnel intersected by normal fault rupture in sand", *Comput. Geotech.*, **111**(7), 137-146. https://doi.org/10.1016/j.compgeo.2019.03.010.

Cai, Q.P. and Ng, C.W.W. (2013), "Analytical approach for

estimating ground deformation profile induced by normal faulting in undrained clay", *Can. Geotech. J.*, **50**(4), 413-422. https://doi.org/10.1139/cgj-2012-0145.

Caulfield, R.J., Kieffer, D.S., Tsztoo, D.F. and Cain, B. (2005), "Seismic design measures for the retrofit of the Claremont tunnel", *Proceedings of the Rapid Excavation and Tunneling Conference*. Colorado, USA.

Cole, D.A. and Lade, P.V. (1984), "Influence zones in alluvium over dip-slip faults", *J. Geotech. Eng.*, **110**(5), 599-615. https://doi.org/10.1061/(ASCE)0733-9410(1984)110:5(599).

Cui, Z., Wang, T.Q., Sheng, Q. and Zhou, G. (2023), "Investigation of the behavior of a tunnel subjected to strike-slip fault rupture with experimental approach", *Geomech. Eng.*, **33**(5), 477-486. https://doi.org/10.12989/gae.2023.33.5.477.

Del Amo, A., Goodfellow, R., Awad, M. and Yang, B. (2018), "Evaluation of a segmental tunnel lining response to a strike slip fault rupture", *Proceedings of the North American Tunneling Conference 2018*, Washington, DC, USA.

Eisenberg, Y. and Treadwell, D.D. (1982), "San Francisco's southwest ocean outfall", *Proceedings of 18th International Conference on Coastal Engineering*. Cape Town, South Africa.

Fan, L., Chen, J.L., Peng, S.Q., Qi, B., Zhou, Q. and Wang, F. (2020), "Seismic response of tunnel under normal fault slips by shaking table test technique", *J. Central South Univ.*, **27**(4), 1306-1319. https://doi.org/10.1007/s11771-020-4368-0.

Gao, J.Q., Wang, Q.Y., Ma, W.G. and Lu, J. (2024), "Failure analysis and comparative study on tunnels under strike-slip fault and oblique-slip fault movements", *Eng. Fail. Anal.*, **164**, 108676. https://doi.org/10.1016/j.engfailanal.2024.108676.

Huang, J.Q., Zhao, M. and Du, X.L. (2017), "Non-linear seismic responses of tunnels within normal fault ground under obliquely incident P waves", *Tunn. Undergr. Sp. Tech.*, **61**, 26-39. https://doi.org/10.1016/j.tust.2016.09.006.

Jalali, M. (2018), "Tunnel rehabilitation in fault zone using sequential joints method-case study: Karaj water conveyance tunnel", *Int. J. Min. Geo-Eng.*, **52**(1), 87-94. https://doi.org/10.22059/ijmge.2018.66155.

Kiani, M., Akhlaghi, T. and Ghalandarzadeh, A. (2016a), "Experimental modeling of segmental shallow tunnels in alluvial affected by normal faults", *Tunn. Undergr. Sp. Tech.*, **51**, 108-119. https://doi.org/10.1016/j.tust.2015.10.005.

Kiani, M., Ghalandarzadeh, A., Akhlaghi, T. and Ahmadi, M. (2016b), "Experimental evaluation of vulnerability for urban segmental tunnels subjected to normal surface faulting", *Soil Dyn. Earthq. Eng.*, **89**, 28-37. https://doi.org/10.1016/j.soildyn.2016.07.012.

Kim, N.Y., Park, D.H., Jung, H.S. and Kim, M.I. (2020), "Deformation characteristics of tunnel bottom after construction under geological conditions of long-term deformation", *Geomech. Eng.*, **21**(2), 171-178. https://doi.org/10.12989/gae.2020.21.2.171.

Konagai, K., Numada, M., Zafeirakos, A., Johansson, J., Sadr, A. and Katagiri, T. (2005), "An example of landslide-inflicted damage to tunnel in the 2004 Mid-Niigata Prefecture earthquake", *Landslides*, **2**(2), 159-163. https://doi.org/10.1007/s10346-005-0057-1.

Lai, J., He, S., Qiu, J., Chen, J., Wang, L., Wang, K. and Wang, J. (2017), "Characteristics of seismic disasters and aseismic measures of tunnels in Wenchuan earthquake", *Environ. Earth Sci.*, **76**(2), 76-94. https://doi.org/10.1007/s12665-017-6405-3.

Lin, M.L., Chung, C.F., Jeng, F.S. and Yao, T.C. (2007), "The deformation of overburden soil induced by thrust faulting and its impact on underground tunnels", *Eng. Geol.*, **92**(3-4), 110-132. https://doi.org/10.1016/j.enggeo.2007.03.008.

Lin, M.L., Chung, C.F. and Jeng, F.S. (2006), "Deformation of overburden soil induced by thrust fault slip", *Eng. Geol.*, **88**(1-2), 70-89. https://doi.org/10.1016/j.enggeo.2006.08.004.

Liu, X.Z., Li, X.F., Sang, Y.L. and Lin , L. (2015), "Experimental study on normal fault rupture propagation in loose strata and its impact on mountain tunnels", *Tunn. Undergr. Sp. Tech.*, **49**, 417-425. https://doi.org/10.1016/j.tust.2015.05.010.

Liu, N., Huang, Q., Wang, L., Fan, W., Jiang, Z. and Peng, J. (2018), "Dynamic characteristics research of a ground fissure site at Xi'an. China", *Tunn. Undergr. Sp. Tech.*, **82**, 182-190. https://doi.org/10.1016/j.tust.2018.08.044.

Liu, Y.Q., Yao, C.F., Luo, W., He, C., Sun, M., Wang, E. and Yuan, F. (2024), "Deformations and damages of tunnels subjected to strike-slip faulting: Effects of tectonic stress and cross-sectional shape", *Eng. Fail. Anal.*, **160**, 108159. https://doi.org/10.1016/j.engfailanal.2024.108159.

Li, P. (2009), "Research on anti-breaking structural design of the highway tunnel across active fault zones", Ph.D. Dissertation, Chongqing Jiaotong University, Chongqing (In Chinese).

Loukidis, D., Bouckovalas, G.D. and Papadimitriou, A.G. (2009), " Analysis of fault rupture propagation through uniform soil cover", *Soil Dyn. Earthq. Eng.*, **29**, 1389-1404. https://doi.org/10.1016/j.soildyn.2009.04.003.

Roy, N. and Sarkar, R. (2017), "A review of seismic damage of mountain tunnels and probable failure mechanisms", *Geotech. Geol. Eng.*, **35**, 1-28. https://doi.org/10.1007/s10706-016-0091-x.

Russo, M., Germani, G. and Amberg, W. (2002), "Design and construction of large tunnel through active faults: a recent application", *Proceedings of International Conference of Tunnelling and Underground Space Use*, Istanbul, Turkey.

Sabagh, M. and Ghalandarzadeh, A. (2020), "Centrifugal modeling of continuous shallow tunnels at active normal faults intersection", *Transport. Geotech.*, **22**, 100325. https://doi.org/10.1016/j.trgeo.2020.100325.

Shahidi, A.R. and Vafaeian, M. (2005), "Analysis of longitudinal profile of the tunnels in the active faulted zone and designing the flexible lining (for Koohrang-III tunnel)", *Tunn. Undergr. Sp. Tech.*, **20**(3), 213-221. https://doi.org/10.1016/j.tust.2004.08.003.

Shen, Y.S., Wang, Z.Z., Yu, J., Zhang, Z. and Gao, B. (2020), "Shaking table test on flexible joints of mountain tunnels passing through normal fault", *Tunn. Undergr. Sp. Tech.*, **98**, 103299. https://doi.org/10.1016/j.tust.2020.103299.

Shen, Y.S., Gao, B., Yang, X.M. and Tao, S. (2014), "Seismic damage mechanism and dynamic deformation characteristic analysis of mountain tunnel after Wenchuan earthquake", *Eng. Geol.*, **180**, 85-98. https://doi.org/10.1016/j.enggeo.2014.07.017.

Sun, F., Zhang, Z.Q. and Yi, Z.W. (2019), "Model experimental study on the influence of normal fault with stick-slip dislocation on the structure of subway tunnel", *Rock Soil Mech.*, 40(8), 3037-3044. https://doi.org/10.16285/j.rsm.2018.1225.

Tali, N., Lashkaripour, G.R., Moghadas, N.H. and Ghalandarzadeh, A. (2019), "Centrifuge modeling of reverse fault rupture propagation through single-layered and stratified soil", *Eng. Geol.*, **249**, 273-289. https://doi.org/10.1016/j.enggeo.2018.12.021.

Wang, W,L., Wan,g T.T., Su, J.J., Lin, C.H. and Seng, C.R. (2001), "Assessment of damage in mountain tunnels due to the Taiwan Chi-Chi Earthquake", *Tunn. Undergr. Sp. Tech.*, **16**(3), 133-150. https://doi.org/10.1016/s0886-7798(01)00047-5.

Wang, Z.F., Shen, S.L., Cheng, W.C. and Su, Y.S. (2016), "Ground fissures in Xi'an and measures to prevent damage to the Metro tunnel system due to geohazards", *Environ. Earth Sci.*, **75**, 1-11. https://doi.org/10.1007/s12665-015-5169-x.

Wang, Z.G., Tao, L.J., Shi, C., An, S. and Liu, J. (2023), "Response and failure mechanism of utility tunnel with flexible joints under reverse fault: An experimental, numerical, and analytical investigation", *Earthq. Spectra*, **39**(1), 335-361.

https://doi.org/10.1177/87552930221143144.

Yan, G.M., Shen, Y.S., Gao, B., Zheng, Q., Fan, K. and Huang, H. (2020), "Damage evolution of tunnel lining with steel reinforced rubber joints under normal faulting: An experimental and numerical investigation", *Tunn. Undergr. Sp. Tech.*, **97**, 103223. https://doi.org/10.1016/j.tust.2019.103223.

Yan, G.M., Zhao, B.M., Wang, Z.J. and Bao, B. (2022), "Simplified analytical solution for responses of fault-crossing tunnels with flexible joints under fault movement", *Structures*, **45**, 984-998. https://doi.org/10.1016/j.istruc.2022.09.054.

Yao, C.F., Duan, J.N., Liu, Y.L., Luo, W., He, C., Yang, W., Zhang, J. and Su, G. (2025), "Damage and failure analysis of twin tunnels with cross passages subjected to strike-slip faulting", *Eng. Fail. Anal.*, **169**, 109197. https://doi.org/10.1016/j.engfailanal.2024.109197.

Yuan, Y., Yu, H.T., Su, Q., Yan, X. and Li, C. (2018), "Multi-point shaking table test for long tunnels subjected to non-uniform seismic loadings–Part I: Theory and validation", *Soil Dyn.. Earthq. Eng.*, **108**, 177-186. https://doi.org/10.1016/j.soildyn.2016.08.017.

Yu, H.T., Yan, X., Bobet, A., Yuan, Y., Xu, G. and Su, Q. (2018a), "Multi-point shaking table test of a long tunnel subjected to non-uniform seismic loadings", *Bull. Earthq. Eng.*, **16**(2), 1041-1059. https://doi.org/10.1007/s10518-017-0223-6.

Yu, H.T., Yuan, Y., Xu, G.P., Su, Q., Yan, X. and Li, C. (2018b), "Multi-point shaking table test for long tunnels subjected to non-uniform seismic loadings - part II: Application to the HZM immersed tunnel", *Soil Dyn. Earthq. Eng.*, **108**, 187-195. https://doi.org/10.1016/j.soildyn.2016.08.018.

Yu, H.T., Chen, J.T., Bobet, A. and Yuan, Y. (2016), "Damage observation and assessment of the Longxi tunnel during the Wenchuan earthquake", *Tunn. Undergr. Sp. Tech.*, **54**, 102-116. https://doi.org/10.1016/j.tust.2016.02.008.

Yu, H.T., Yuan, Y., Liu, X., Li, Y.W. and Ji, S.W. (2013), "Damages of the Shaohuoping road tunnel near the epicentre", *Struct. Infrastruct. Eng.*, **9**(9), 935-951. https://doi.org/0.1080/15732479.2011.647038.

Zaheri, M., Ranjbarnia, M. and Dias, D. (2020), "3D numerical investigation of segmental tunnels performance crossing a dip-slip fault", *Geomech. Eng.*, **23**(4), 351-364. https://doi.org/10.12989/gae.2020.23.4.351.

Zhang, X.P., Jiang, Y.J., Hirakawa, Y., Cai, Y. and Sugimoto, S. (2019), "Correlation between seismic damages of Tawarayama tunnel and ground deformation under the 2016 Kumamoto Earthquake", *Rock Mech. Rock Eng.*, **52**(7), 2401-2413. https://doi.org/10.1007/s00603-018-1704-x.

Zhang, X., Yu, L., Wang, M.N. and Yang, H. (2024), "Mechanical response and failure characteristics of tunnels subjected to reverse faulting with nonuniform displacement: Theoretical and numerical investigation", *Eng. Fail. Anal.*, **156**, 107809. https://doi.org/10.1016/j.engfailanal.2023.107809.

Zhao, M., Xu, L.H., Huang, J.Q., Du, X. and Li, H. (2023), "Analytical solutions of the tunnels under the fault creeping by elastic foundation beam model with considering tangential interaction", *Soil Dyn. Earthq. Eng.*, **172**, 108047. https://doi.org/10.1016/j.soildyn.2023.108047.

Zhao, K., Chen, W.Z., Yang, D.S., Zhao, W.S., Wang, S. and Song, W. (2019), "Mechanical tests and engineering applicability of fibre plastic concrete used in tunnel design in active fault zones", *Tunn. Undergr. Sp. Tech.*, **88**, 200-208. https://doi.org/10.1016/j.tust.2019.03.009.

Zeng, G.X., Geng, P., Guo, X.Y., Li, P., Wang, Q. and Ding, T. (2021), "An anti-fault study of basalt fiber reinforced concrete in tunnels crossing a stick-slip fault", *Soil Dyn. Earthq. Eng.*, **148**, 106687. https://doi.org/10.1016/j.soildyn.2021.106687.

Zhong, Z.L., Wang, Z., Zhao, M. and Du, X. (2020), "Structural damage assessment of mountain tunnels in fault fracture zone subjected to multiple strike-slip fault movement", *Tunn. Undergr. Sp. Tech.*, **104**(10), 103527. https://doi.org/10.1016/j.tust.2020.103527.

CG